**ZESZYTY NAUKOWE
SCIENTIFIC JOURNAL
264**

ELEKTROTECHNIKA

ELECTRICAL
ENGINEERING

17

Contents

MULTITRANSDUCER WITH FREQUENCY OUTPUT FOR COMPUTERIZED MEASUREMENT SYSTEM APPLICATION

Tomasz Marek Jaczyński

University of Technology and Life Sciences
al. prof. S. Kaliskiego 7, 85-796 Bydgoszcz
tomasz.jaczynski@utp.edu.pl

Summary: This paper presents a Multitransducer with frequency output for computerized measurement system application. It describes the construction of the Multitransducer for the measurement of single-phase loads. Metrological properties were examined and analyzed for the implemented system. Finally a multitransducers didactic and practical usefulness have been discussed.

Keywords: multitransducer, transducer, method of least squares, analysis of the metrological property, measuring system computerized, LabVIEW

1. INTRODUCTION

Currently, it is necessary to analyse multiple electrical quantities. For this purpose, multitransducers that consist of integrated transducers for different single electrical signals are most commonly used. On its outputs, the multitransducer generates standard voltage or current signals, depending on the type of device. Additionally multitransducers possess the transmission ports (RS232, USB), which can transfer the measured values via transmission protocol directly to your PC. In the computerized measurement system the most common way to convert analog signals to digital form is via measurement card, which allows to readi, collect and process the data. One of the unconventional approaches is to use the multitransducer with frequency outputs. In this type of device, we get the opportunity to make simple isolation for safe analysis. The measurement is dangerous when the device is powered with mains voltage, ie. 230V AC. An important fact is that the signals levels on frequency outputs are usually compatible with TTL. This allows connecting them directly to a PC. With this solution, the obtained measurement system is cheaper, less complex and does not require the use of a measuring card. This results in greater reliability of such a measurement system. Therefore, it is reasonable to create a multitransducer with frequency outputs for single-phase loads electrical parameters. In addition, it is recommended that this device should usea small number of components, with a relatively simple and compact design. The miniaturization of the device improves its dynamic performance and stability. Nowadays the miniaturization is an integral part of any modern device structures.

2. CONSTRUCTION OF MULTITRANSDUCER
FOR SINGLE- PHASE LOADS MEASUREMENT

The multitransducer consists of four blocks for conversion of measured values in the time-frequency signals (Figure 1), which allows processing of electrical parameters such as:

- active power consumed by the receiver,
- supply voltage,
- the current flowing through the receiver,
- phase shift between voltage and current.

In order to minimize the number of components, following processing constant coefficients were used:

- 10 Hz for 1 W of active power P (range 0-300 W),
- 10 Hz for 1 V of true voltage value URMS (range 200-250 V),
- 3 Hz for 0.1 mA of true value of the current IRMS (range 0-130 mA) or 3 Hz for 1 mA (range of 0-1.3 A),
- 20 Hz for 1° of the phase shift angle (range 0-90 °).

The structure of the measuring system was based on the author's experience with similar types of systems. Naturally other solutions were considered, but their prototypes were crucial for finding defects and allowed to choose a solution from the first picture.

Converter block for the active power consumed by the pulse frequency converter is based mainlyon the AD7755 chip, which is a comprehensive solution which provides the desired effect. This system allows miniaturization of the multitransducer. Thanks to this, it is possible to omit the following functional blocks of the converter:

- block for processing sinusoidal voltage and current signals to their rms values,
- multiplication block for signals comprising the active power,
- voltage to frequency converter block.

Function blocks described above are digitally implemented by AD7755. It is very convenient that by using this system there is no need to calibrate individual analog blocks. The AD7755 usage is a compromise between fixed errors caused by the conversion of the current and voltage signal into digital form via a built-in ADC, and the lack of need for laborious calibration. The production of the applied system has been discontinued, but due to its very good properties it continues to be used. He lived to see its own copy with the same BL6503S parameters. AD7755 system and BL6503S in this unit behave virtually identically. The differences are negligible, as in the case of the same circuits with different production batches. Analog Devices company now offers systems similar to AD7755, and even better, but the drawback would be the service speed of SPI. This type of serial communication enforces the need for a microcontroller which, overall, could become a more expensive solution than the proposed one.
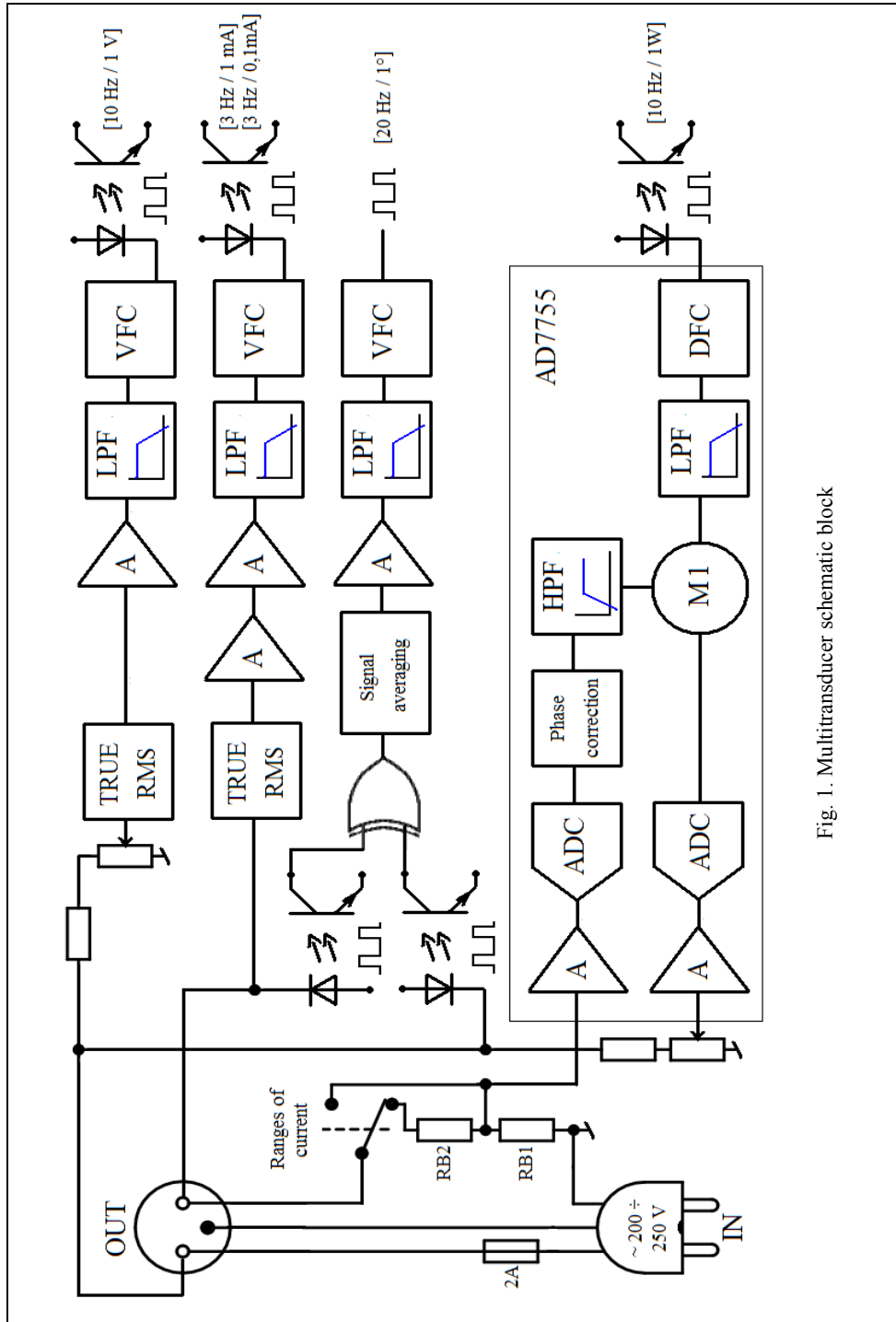
Fig. 1. Multitransducer schematic block

Multitransducer module which is responsible for processing the voltage (230 V AC) to a frequency signal has been designed with low complexity and very good parameters. Due to this, it consists of a voltage divider, from which the output signal goes to the rms value of TRUE RMS AD736 transducer. Signal outputted from AD736 transducer is conditioned and filtered for the last part of the processing, which is the LM331 chip. It serves as a converter of voltage signal into frequency signal. The resulting signal conversion module is provided for processing a signal voltage between 0 V and 250 V TRUE RMS. Unfortunately, for miniaturization of multitransducer purpose, the processed voltage is also a power supply voltage. Therefore, it can be safely assumed that effective voltage range of the processed signal should range from 200 V to 250 V.

Block for processing the current drawn to frequency pulses is created in a similar way as the voltage processing block. Its primary difference is that it has a more powerful amplification-processing system, where the voltage signal coming from the shunt requires greater attention due to the very low values and the necessity to process current value from 0 mA. In a situation where the processed quantity can take a zero value, it is advisable to raise its signal level. In the designed block, the output frequency signal for 0 mA is 1 kHz. In order to obtain higher processing resolution, two ranges of current drawn by the receiver were introduced. The first scope covers values from 0 mA to 130 mA, and the second from 0 mA to 1300 mA. The ranges are changed by a switch that turns the relay on or off, by which the measurement shunt value is changed. The resistor value 0.3 Ω 1% is used to measure the current in the range up to 1300 mA, and the shunt value of 3 Ω 1% is dedicated to the range below 130 mA.

The converter module of phase angle into frequency pulses is mainly based on a classical EX-OR logic gate. The rectangular signal representing the supply voltage and the rectangular signal representing the current are connected to the two inputs of the gate. In order to convert the sine wave into a square wave signal, an optocoupler is used, in which the LED is fed through resistors directly from the mains voltage. Square wave signal corresponding to the level of the current is formed with the use of the comparator, which works as a detector of crossing 0 V by voltage signal coming from the measurement shunt. Thanks to the level regulation of the comparator switching, a threshold can be selected for which the device will work properly with both very low and high current consumption. Subsequently, the signal from the operational amplifier working as a comparator is applied to the optocoupler. The signal on the gate output is in pulse width modulation, which is generally called a PWM signal. That signal is averaged, amplified and filtered accordingly. Thus prepared, the signal is indicated on the LM331 transmitter circuit, whose function is to convert the voltage signal into a frequency signal. In this conversion block, similarly as in the current to frequency conversion, an increase of frequency value for lack of phase shift is used. Therefore, for a value of 0 °, the frequency output value will be 1 kHz. The developed solution is not complicated and at the same time satisfying due to the diligent choice of elements for the proper calibration of optocouplers.

In a comprehensive solution that is the multitransducer, a power supply is necessary. Multitransducer processing accuracy will largely depend on the design of its power supply. In the case of the proposed device, voltage of +/- 5 V and isolated voltage +5 V was required. It is important to note that the power needed for the design must be stable over time, have a low output voltage ripple, and the value of voltage

can not vary over time. Additionally, due to multitransducer power supply voltage between 200-250 V AC, power supply systems also have to ensure the stability of the parameters. To obtain a stable voltage +/- 5 V linear circuits stabilizers L7805CV and L7905CV were applied. The resulting voltages are not isolated from the mains supply since the systems forming and processing signals required such a solution. This means that the potential of 0 V (GND) is equivalent to the potential of the neutral N in the mains. Therefore, to ensure safety, all outputs of the individual signal processing blocks are isolated by optocouplers. For properly carrying the signals through optocouplers, safe voltage +5 V was used on the user side. For an isolated +5 V voltage integrated DC / DC converters AM1D0505SZ (Aimtec) powered from not isolated -5 V were applied.

The described processing blocks with multitransducers power form an electronic device which equals its parameters with currently produced multitransducers of this type. During the start of the designed device, it is important to make a thorough calibration of all possible settings of function blocks, in order to minimize signal-processing errors.

3. RESEARCH AND ANALYSIS OF THE METROLOGICAL CHARACTERISTICS OF THE REALIZED DEVICE

To perform examination of multitransducer (Fig. 2) a measurements system consisted of the following components has been set up:
- oscilloscope GDS-1022 GWINSTEK,
- frequency counter U2000 PROTEK,
- laboratory autotransformer AL-2500,
- wattmeter LW-1,
- ammeter TLEM-2,
- digital voltmeter BM805 BRYMEN,
- adjustable resistor with a value of 770 Ω OL2/400,
- light bulb 100 W,
- light bulb with switch 100 W,
- multiransducer,
- one-phase receiver RLC.

This allowed the system to calibrate all processing channels of the multitransducer. Tuning accuracy will depend on the adopted method of measurement and the measuring instruments. Calibration for each channel took place in the middle or near the middle of the processing range of every individual transducer. This procedure allowed to show the non-ideal linearity of processing characteristics Verification of the calibration process is made by the least squares method. For this purpose, it was necessary to perform measurements. Number of the measurements points is very important, because it affects the accuracy of determining the processing characteristics of the transducers.
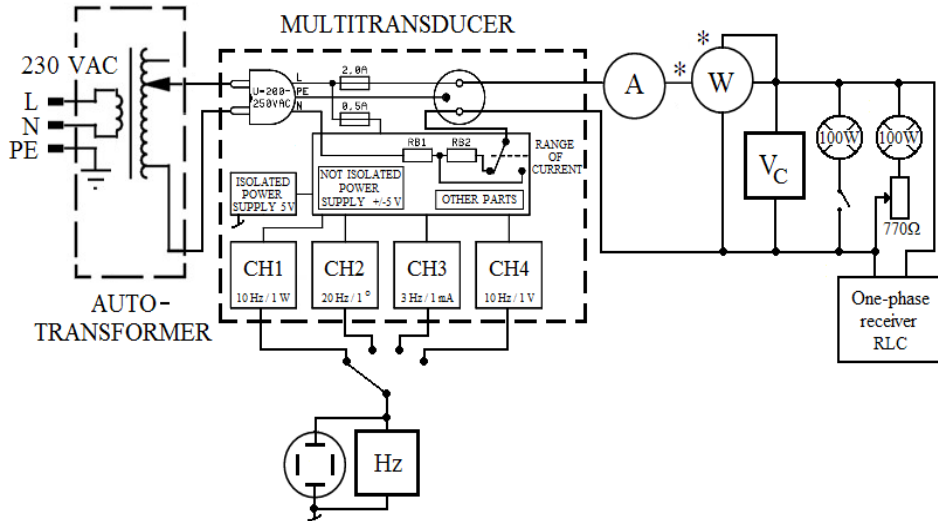
Fig. 2. Schematic of the measurement experiment of the multitransducer

The general mathematical model of the curve, used to determine the functional relationship between the input and the output of individual channel of the multitranscuders, is as follows:

$$\hat{Y} = f(X) \tag{1}$$

where:

X – the value of input transducer,

$\hat{Y}$ – the value of output transducer.

The least squares method is used to determine the regression line, which symbolizesthe functional processing relationship of each channel of the multitransducer. This article presents in-depth analysis of one processing path for measurements and least squares method. Other channels of the multitransducer are shortly reviewed and judged on their usefulness.

The multitransducer functions properly when the processed voltage ranges from 200 V to 250 V. Due to the use of LM331 transducers, which average the signal at its output, there is no need for a voltage stabilizer during the test. This was confirmed by repeatedly testing the same value in a randomly varying intervals of time. Table 1 shows the results of setting the voltage, measurement frequency, calculated processed constant for a given measurement. Additionally, the following table shows the absolute and relative errors relating to the predetermined processing constant of 10 Hz/V.

Table 1. Results of measurements and calculations for „voltage – frequency" channel

U (V)	f (Hz)	f/U (Hz/V)	$\Delta f/U$ (Hz/V)	$\delta f/U$ (%)
200,2	2017	10,07	0,07	0,75
205,3	2064	10,05	0,05	0,54
210,2	2114	10,06	0,06	0,57
215,0	2161	10,05	0,05	0,51
220,1	2214	10,06	0,06	0,59
225,4	2262	10,04	0,04	0,35
230,4	2318	10,06	0,06	0,61
235,4	2373	10,08	0,08	0,81
240,0	2420	10,08	0,08	0,83
245,0	2468	10,07	0,07	0,73
250,0	2527	10,10	0,10	0,96

Basing on the results from Table 1, a regression curve of the transducer was calculated by least squares method. Figure 3 shows a graph in which, aside from the specific points of processing, the regression curve of the transducer was also presented (voltage to frequency).

For the other processing channels metrological analysis was conducted in the same manner, with the results of a satisfactory level. Because of its low complexity, the voltage to frequency transducer turned out to be of a very good quality.
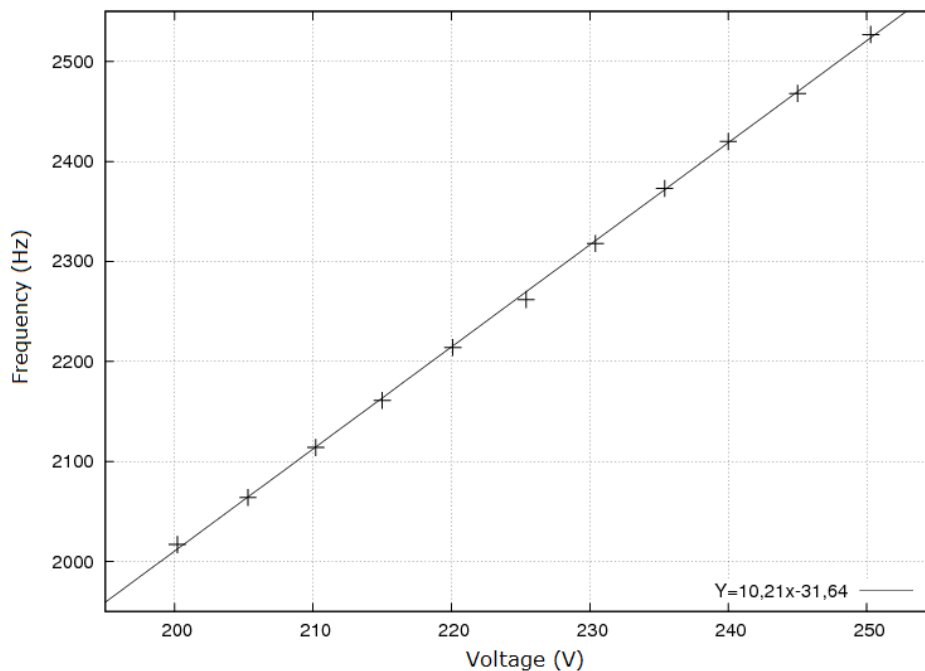

Fig. 3. Graph of the transducer – voltage to frequency

An important fact is the use of voltage-to-frequency LM331 converters, which results in averaging output signals. However, after the analysis of the projected measurement, it was concluded that it has no impact in the context of the measurement of static values.

4. COMPUTERIZED MEASUREMENT SYSTEM WITH PRESENT MULTITRANSDUCER

Multitransducer has been integrated into the modern measuring system whose additional components were a "frequency – code" multi-converter and a PC with LabVIEW software installed. The block diagram of the system is shown in Figure 4.

The application written in LabVIEW allows to simultaneously read from four outputs of the multitransducer. The screenshot of the running application is shown in Figure 5. The software allows to enter the regression coefficients for the given channel of multitransducer via the least squares method. The way of a specific channel processing curve change is determined by mathematical formula for the quadratic function:

$$Y = Ax^2 + Bx + C \tag{2}$$

where:

    Y – value of the function,
    x – argument of a function,
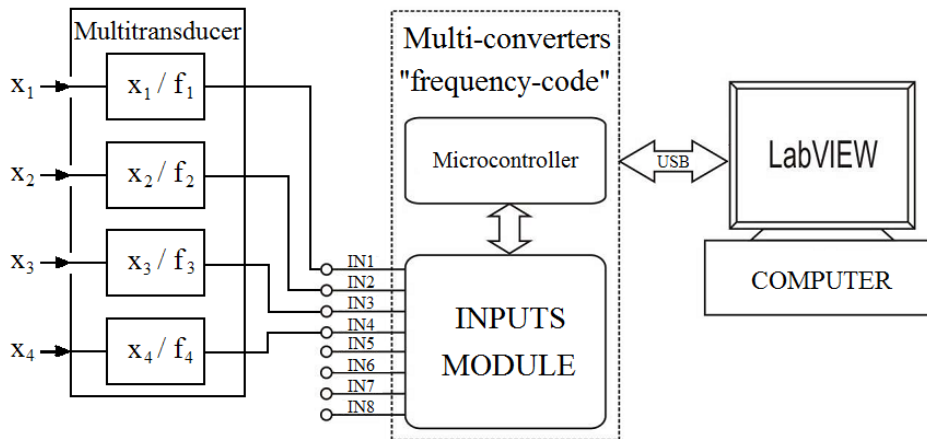 A, B, C – coefficients.

Fig. 4. Computerized measurement system block diagram

This solution saves time spent on writing or correcting the measurement system software when change of multitranscuder design is needed. The resulting processing characteristics of all channels in the device are linear and therefore the A coefficient equals zero.
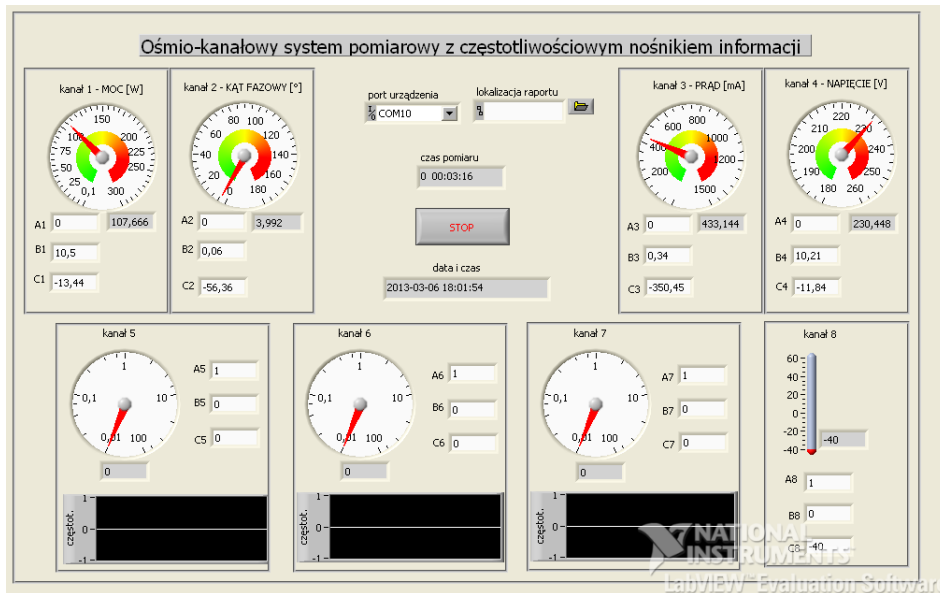
Fig. 5. Application for computerized measurement system

The measurement values were taken via Computerized measuring system, which aimed to examine the mapping error of values measured by different measuring instruments. For example, consider the voltage measurement, when the measurement of both absolute and relative error does not have a clear character, as shown in Table 2. The worst value of the relative error is 1%, which is classifies the method as a promising one.

Table 2. Results of the measurement of the voltage True value RMS and the errors

Ur (V)	Um (V)	ΔU (V)	δU (%)
200,0	200,53	0,53	0,27
210,0	210,51	0,51	0,24
220,0	221,47	1,47	0,67
230,0	231,44	1,44	0,63
240,0	242,41	2,41	1,00
250,0	252,38	2,38	0,95

where: Ur – value of reference voltage, Um – value of measure voltage, ΔU – absolute error voltage, δU – relative error voltage.

The reference voltage value is read from the class 0.5% voltmeter and the measured voltage is the result of a computer readout of the measurement system.

Others processing channels of multitransducer unfortunately fared worse, which means that the number of performed calibrations was insufficient or that the multitransducer requires minor adjustments to its design.

However, it is worth noting that the above test results were performed for different lengths of wires sending the frequency signals. The results did not differ between connection one meter long and the ones one hundred meter long, which proves that the described multitransducer performs its role well.

5. CONCLUSIONS

The multitransducer presented in this article has a large potential for both educational and practical purpose. It shows a lot of metrological dependencies in the individual processing channels. At the present time, the multitransducer is used in the computer system presented in section four, as a laboratory exercise in "Computerized measurement system" classes. If the processing channels were further refined, in such a way, that the values of processing errors and errors resulting from the values read from the measuring computer system were the same or better than the processing error of voltage to frequency transducer, this entire device would be so attractive that it could compete with the solutions currently available for purchase. It could not only match or even exceeded its accuracy class, but its price would be attractive as well. Total price of the components of the multitransducer described above should not exceed 300 PLN, considering the multitransducers prices that range from about 2000 PLN to 5000 PLN. This multitransducer has a chance to become an alternative for expensive solutions which are currently on the market. While summarizing the metrological properties of the multitransducer, it is important to use a maximum number of calibration steps for each block, so that we can achieve the maximum accuracy of the processed values.

Transducers with frequency output can be a solution for the future because of their versatility and flexible application. One of the many possible stages of development of the described issue, are fully programmable multitransducers that will supersede dedicated solutions, such as those described in the article. However, the price of the dedicated solutions will always be lower, so it will be reasonable to create multitransducers like the one discussed in this publication.

BIBLIOGRAPHY

[1] Chwaleba A., Poniński M., Siedlecki A., 2003. Metrologia elektryczna. Wydawnictwo Naukowo-Techniczne Warszawa.
[2] Derlecki S., 2005. Metrologia elektryczna i elektroniczna. Wydawnictwo Politechniki Łódzkiej.
[3] Piotrowski J., Kostyrko K., 2000. Wzorcowanie aparatury pomiarowej, PWN Warszawa.
[4] Czajewski J., 2004. Podstawy metrologii elektrycznej. Oficyna Wydawnicza Politechniki Warszawskiej.
[5] Jasik J.R., 2003. Przetwarzanie sygnałów pomiarowych w systemach z częstotliwościowym nośnikiem informacji, Wydawnictwo Politechniki Lubelskiej.

[6] Borowicz J., Nitz Ł., 2012. Równoczesne komputerowe pomiary częstotliwości szeregu sygnałów impulsowych. Dyplomowa praca magisterska, UTP – WTIE Bydgoszcz.

[7] Jaczyński T., 2013. Konwertery z wyjściami częstotliwościowymi parametrów elektrycznych odbiorników jednofazowych zasilanych z sieci energetycznej (projekt i realizacja). Dyplomowa praca magisterska, UTP – WTIE Bydgoszcz.

MULTIPRZETWORNIK Z WYJŚCIAMI CZĘSTOTLIWOŚCIOWYMI DO ZASTOSOWAŃ W KOMPUTEROWYM SYSTEMIE POMIAROWYM

Streszczenie

W pracy omówiono multiprzetwornik z wyjściami częstotliwościowymi do zastosowań w komputerowym systemie pomiarowym. Opisano budowę multiprzetwornika realizującego pomiar parametrów odbiorników jednofazowych, a także dokonano badania oraz analizę właściwości metrologicznych zrealizowanego układu. Finalnie omówiono przydatność opisywanego multiprzetwornika pod kątem dydaktycznym oraz praktycznym.

Słowa kluczowe: multiprzetwronik, przetwornik pomiarowy, metoda najmniejszych kwadratów, analiza własności metrologicznych, komputerowy system pomiarowy, LabVIEW

APPLYING THE METHOD OF AVERAGE VOLTAGE ON THE INTEGRATION STEP LENGTH FOR THE ANALYSIS OF ELECTRICAL CIRCUITS

Zbigniew Kłosowski, Omelian Płachtyna, Piotr Grugel

University of Technology and Life Sciences
al. prof. S. Kaliskiego 7, 85-796 Bydgoszcz
klosowski@utp.edu.pl; plakht@utp.edu.pl; Piotr.Grugelt@utp.edu.pl

Summary: The paper presents the analysis of complex circuits using the method of average voltage on the integration step length. An algorithm is presented to solve complex circuits with the given method. The paper also compares the time of determination of numerical solution between this solution and the exact solution using various methods with predetermined error. This comparison is used to determine the suitability (effectiveness) of the method to analyze complex circuits.

Keywords: analysis of electrical circuits, a method of average voltage on the integration step length, compare the complexity of numerical integration methods

1. INTRODUCTION

The analysis of electric circuits in the time domain involves the determination of voltage and transient currents occurring in the system. In order to carry out an analysis, usually a complex system of ordinary differential equations needs to be solved. In the majority of the considered issues these equations cannot be solved analytically, therefore, numerical methods must be used in order to obtain a solution. This poses a question of which numerical integration method should be used. To solve this problem, a comparison of method of average voltage on the integration step length with conventional methods based on the electrical circuit DC and AC needs to be made.

Based on the simulation results, it was determined that the fastest way of obtaining the solution for the given medium-sized circuits is the method of average voltage on the integration step length.

2. GENERAL DESCRIPTION OF THE METHOD OF AVERAGE VOLTAGE ON THE INTEGRATION STEP LENGTH

In electrical circuits a single branch may contain resistors, capacitors, inductors and power supplies. The circuit branch containing all these elements is shown in Fig. 1.
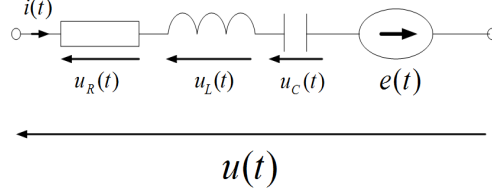
Fig. 1. Branch of an electric circuit

The essence of the method of average voltage on the integration step length is algebraization of differential equations [8] which leads to electrical circuit (Fig. 1) forming a branch of the serial combined electromotive force E_S and equivalent resistance R_S (Fig. 2).
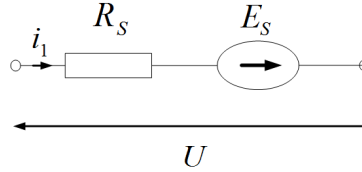
Fig. 2. Equivalent diagram of the voltage circuit for the method of average voltage on the integration step length of the m-th degree

Branch terminals shown in Fig. 2 have an U voltage value, which is the average voltage at the integration step. E_S and R_S values for the method of average voltage on the integration step length of the m-th degree are calculated from the relation:
–   equivalent electromotive force E_S [V]

$$E_S = E - u_{R0} - u_{C0} + \left(\frac{R}{m+1} + \frac{\Delta t}{C} \cdot \frac{2-(m+1)(m+2)}{2(m+1)(m+2)} + \frac{L_0}{\Delta t} \right) \cdot i_0 - $$
$$- \sum_{k=1}^{m-1} \left(\frac{R\Delta t^k}{(k+1)!} \cdot \frac{m-k}{m+1} + \frac{\Delta t^{k+1}}{C(k+2)!} \cdot \frac{(m+1)(m+2)-(k+1)(k+2)}{(m+1)(m+2)} \right) \frac{d^{(k)}i_0}{dt^{(k)}} \tag{1}$$

–   equivalent resistance R_S [Ω]

$$R_S = \frac{R}{m+1} + \frac{\Delta t}{C(m+1)(m+2)} + \frac{L_1}{\Delta t} \tag{2}$$

The current at the end of the integration step is determined by the relation:

$$i_1 = \frac{U + E_S}{R_S} \tag{3}$$

However, in order to determine the voltage across the capacitor at the end of the integration step, the following formula needs to be used:

$$u_{C1} = u_{C0} + \frac{\Delta t}{C(m+1)} \cdot (m \cdot i_0 + i_1) + \sum_{k=1}^{m-1} \frac{\Delta t^{k+1}}{(k+1)!} \cdot \frac{1}{C} \cdot \frac{m-k}{m+1} \frac{\mathrm{d}^{(k)} i_0}{\mathrm{d} t^{(k)}} \qquad (4)$$

Derivation of the above relations is shown in [8] and [9].

The branch of the analyzed circuit (Fig. 1) can also be represented by a current source (Fig. 3), on whose terminals occurs the average voltage on the integration step length. The resistance occurs inside the perimeter of the R_S and the current source $I_1 = E_S/R_S$, which contain information about the parameters and processes in the branch at the end of the integration step.
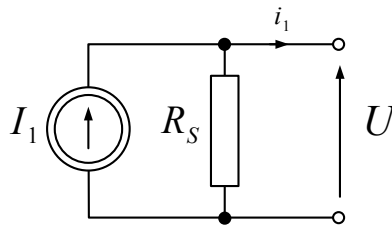
Fig. 3. Equivalent diagram of the current for the method of average voltage on the integration step length of the m-th degree

3. AN EXAMPLE OF THE APPLICATION OF THE DESCRIBED METHOD FOR DC CIRCUIT ANALYSIS

Fig. 4 shows a DC circuit diagram, on basis of which the method of average voltage on the integration step length for analyzing electrical circuits is presented.
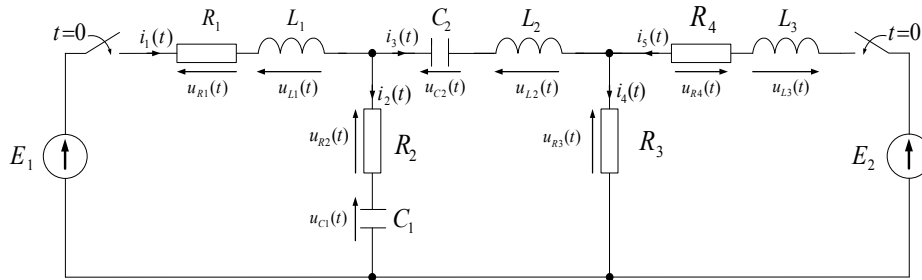
Fig. 4. Diagram of the analyzed DC circuit

While analyzing the electrical circuit (Fig. 4) with the use of the described numerical method, each branch circuit must be replaced by an equivalent serial connection of E_S electromotive force and equivalent R_S resistance. The equivalent electrical circuit diagram under consideration is shown in Fig. 5. Following equations can be written for it on the basis of I and II Kirchhoff's Rights, where the subscript 1 denotes the value at the end of the integration step:

$$R_{S1}i_{11} + R_{S2}i_{21} = E_{S1} + E_{S2}$$

$$R_{S2}i_{21} - R_{S3}i_{31} - R_{S4}i_{41} = E_{S2} - E_{S3} - E_{S4}$$

$$R_{S5}i_{51} + R_{S4}i_{41} = E_{S5} + E_{S4} \tag{5}$$

$$i_{21} = i_{11} - i_{31}$$

$$i_{41} = i_{51} + i_{31}$$
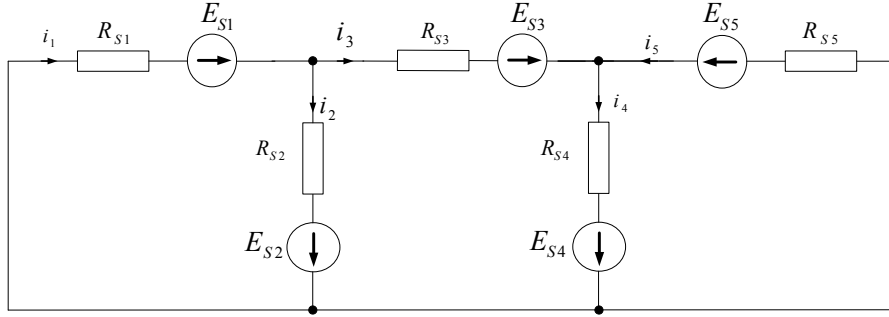
Fig. 5. Equivalent diagram of the analyzed DC circuit

The equations (5) can be written as the following system of equations after putting them in order:

$$\left(R_{S1} + R_{S2}\right)\cdot i_{11} - R_{S2}i_{31} = E_{S1} + E_{S2}$$

$$R_{S2}i_{11} - \left(R_{S2} + R_{S3} + R_{S4}\right)\cdot i_{31} - R_{S4}i_{51} = E_{S2} - E_{S3} - E_{S4}$$

$$R_{S4}i_{31} + \left(R_{S4} + R_{S5}\right)\cdot i_{51} = E_{S5} + E_{S4} \tag{6}$$

$$i_{21} = i_{11} - i_{31} \qquad i_{41} = i_{51} + i_{31}$$

The algorithm for solving the electrical circuit shown in Fig. 5 has been presented for the method of average voltage on the integration step length of the 2nd order of integration step (coefficient m occurring in the general formulas (1), (2) and (4) assumes a value of 2).

1. Determination of the first derivatives at the beginning of the integration step. Derivatives should be recorded on the basis of an electrical circuit diagram shown in Fig. 3 as follows:

$$\frac{\mathrm{d}i_{10}}{\mathrm{d}t} = \frac{E_1 - R_1 i_{10} - R_2 i_{20} - u_{C10}}{L_1}$$

$$\frac{\mathrm{d}i_{30}}{\mathrm{d}t} = \frac{u_{C10} - u_{C20} + R_2 i_{20} - R_3 i_{40}}{L_2}$$

$$\frac{di_{50}}{dt} = \frac{E_2 - R_4 i_{50} - R_3 i_{40}}{L_3}$$

$$\frac{di_{20}}{dt} = \frac{di_{10}}{dt} - \frac{di_{30}}{dt} \; ; \quad \frac{di_{40}}{dt} = \frac{di_{30}}{dt} + \frac{di_{50}}{dt}$$

2. Calculation of the equivalent electromotive ES force. To perform it, use the following formula (1):

$$E_{S1} = E_1 - R_1 i_{10} + \left(\frac{R_1}{3} + \frac{L_1}{\Delta t}\right) \cdot i_{10} - \frac{R_1 \Delta t}{6} \cdot \frac{di_{10}}{dt}$$

$$E_{S2} = -R_2 i_{20} - u_{C10} + \left(\frac{R_2}{3} - \frac{5\Delta t}{12C_1}\right) \cdot i_{20} - \left(\frac{R_1 \Delta t}{6} + \frac{\Delta t^2}{12C_2}\right) \cdot \frac{di_{20}}{dt}$$

$$E_{S3} = -u_{C20} + \left(-\frac{5\Delta t}{12C_2} + \frac{L_2}{\Delta t}\right) \cdot i_{30} - \frac{\Delta t^2}{12C_2} \frac{di_{30}}{dt}$$

$$E_{S4} = -R_3 \cdot i_{40} + \frac{R_3}{3} \cdot i_{40} - \frac{R_3 \Delta t}{6} \cdot \frac{di_{40}}{dt}$$

$$E_{S5} = E_2 - R_4 i_{50} + \left(\frac{R_4}{3} + \frac{L_3}{\Delta t}\right) \cdot i_{50} - \frac{R_4 \Delta t}{6} \cdot \frac{di_{50}}{dt}$$

3. Calculation of the equivalent R_S resistance, using the formula (2):

$$R_{S1} = \frac{R_1}{3} + \frac{L_1}{\Delta t} \; ; \; R_{S2} = \frac{R_2}{3} + \frac{\Delta t}{12C_1} \; ; \; R_{S3} = \frac{\Delta t}{12C_2} + \frac{L_2}{\Delta t} \; ; \; R_{S4} = \frac{R_3}{3} \; ; R_{S5} = \frac{R_4}{3} + \frac{L_3}{\Delta t}$$

4. The solution of equation (6). The current values at the end of the current integration step are obtained on this basis.
5. Determination of voltages on the capacitors at the end of the integration step using the formula (4):

$$u_{C11} = u_{C10} + \frac{\Delta t}{3C_1} \cdot (2 \cdot i_{20} + i_{21}) + \frac{\Delta t^2}{6C_1} \frac{di_{20}}{dt}$$

$$u_{C21} = u_{C20} + \frac{\Delta t}{3C_2} \cdot (2 \cdot i_{30} + i_{31}) + \frac{\Delta t^2}{6C_2} \cdot \frac{di_{30}}{dt}$$

Analysis of the given system (Fig. 3) in the time domain consisted of determining the transient currents $i_1(t)$, $i_2(t)$, $i_3(t)$, $i_4(t)$, i_15t). They are presented in Fig. 6. In order to determine the value of physical items, the following data was used: $E_1 = 100$ V, $E_2 = 50$ V, $R_1 = 20$ Ω, $R_2 = 30$ Ω, $R_3 = 15$ Ω, $R_4 = 1$ Ω, $L_1 = 1$ mH, $L_2 = 3$ mH $L_3 = 2$ mH, $C_1 = 1$ uF, $C_2 = 2$ uF. The transient currents were obtained by solving the system of

equations analytically and numerically with a fixed integration step. The following methods were used: [1, 2, 3, 4, 5, 6, 7, 10]:

- trapezoids (T),
- 2nd order Runge-Kutta ,
- 4th order Runge-Kutta f (RKIV)
- Bogacki-Shampine (BS),
- 4th and 5th order Dormand-Prince (DP54),
- 2nd and 3rd order Runge-Kutta-Fehlberg (RKF23),
- 4th and 5th order Runge-Kutta-Fehlberga(RKF45),
- Adams-Bashfortha row II (ABII),
- 3rd order Adams-Bashfortha (ABIII),
- 4th order Adams-Bashforth (ABIV),
- 2nd order Adams-Moulton-Bashfortha (ABMII),
- 3rd order Adams-Moulton-Bashfortha (ABMIII),
- 4th order Adams-Moulton-Bashforth (ABMIV),
- 3rd order Gear (GIII), 4th order Gear IV (GIV),
- 1st order method of average voltage on the integration step length (NSI)
- 2nd order method of average voltage on the integration step length (NŚII),
- 3rd order method of average voltage on the integration step length (NŚIII).

Obtaining the results of numerical integration methods, it was assumed that the error described in equation (7) between the exact analytical solution (index A) and approximate numerical solution (index *N*) for a given time point, referred to the maximum current value of the analytical solution (index max*A)* will equal 0.500%.

$$\delta_i = \frac{\left| i_A\left(t\right) - i_N\left(t\right) \right|}{\left| i_{max\,A} \right|} 100\% \tag{7}$$
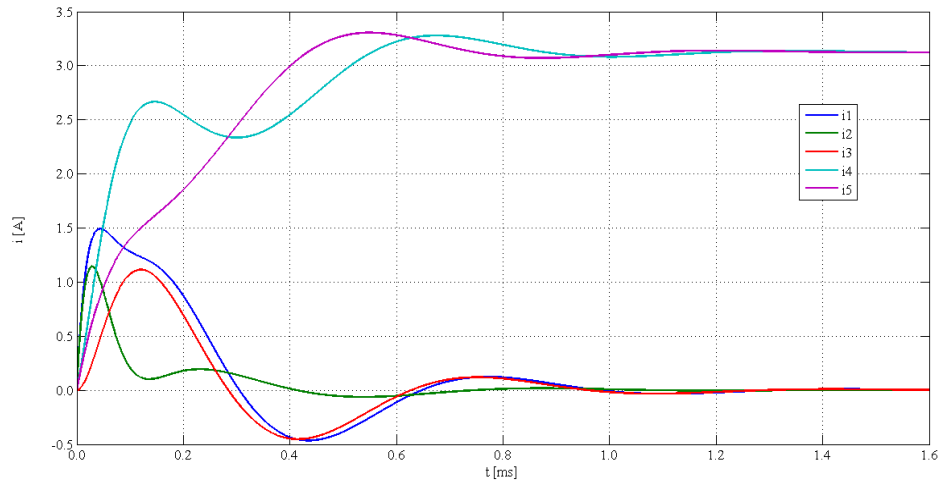

Fig. 6. The analytically designated transient currents flowing in the analyzed DC circuit

Tables 1 and 2 present the results of the analyzed circuit simulation, which inform about how many steps, in the given method, you need to perform during the occurrence of the transient state in order to get a solution with a predetermined maximum error (parameter labeled "number of steps"), and how many calculations you need to perform during the occurrence of the transient state in order to obtain a solution with a predetermined maximum error. This indicates the time of designation, given that the number of calculations is the product of the number of steps in the method which must be performed by the number of coefficients calculated in the method, which are needed to determine the next value ("Calculation volume" parameter).

Table 1. Simulation results for the given DC circuit

No.	Numerical method	Numer of steps	Numer of calculations	δ_{i1} [%]	δ_{i2} [%]	δ_{i3} [%]
1	NŚ III	60	180	0,307	0,500	0,105
2	AB IV	189	189	0,334	0,500	0,085
3	ABM IV	116	232	0,337	0,500	0,083
4	NŚ II	117	234	0,308	0,500	0,099
5	RKF 45	49	294	0,276	0,500	0,142
6	DP 54	49	294	0,333	0,500	0,165
7	AB III	296	296	0,314	0,500	0,102
8	RK IV	77	308	0,345	0,500	0,081
9	T	319	319	0,307	0,500	0,107
10	ABM III	171	342	0,324	0,500	0,082
11	NŚ I	344	344	0,305	0,500	0,108
12	G IV	231	462	0,308	0,500	0,102
13	BS	154	462	0,323	0,500	0,095
14	G III	268	536	0,332	0,500	0,078
15	RKF 23	157	628	0,323	0,500	0,096
16	AB II	715	715	0,313	0,500	0,094
17	ABM II	365	730	0,312	0,500	0,103
18	RK II	472	944	0,314	0,500	0,092
19	G II	693	1386	0,311	0,500	0,103

Table 2. Simulation results for the given DC circuit

No.	Numerical method	Numer of steps	Numer of calculations	δ_{i4} [%]	δ_{i5} [%]
1	NŚ III	60	180	0,033	0,003
2	AB IV	189	189	0,037	0,011
3	ABM IV	116	232	0,035	0,009
4	NŚ II	117	234	0,041	0,003
5	RKF 45	49	294	0,057	0,005
6	DP 54	49	294	0,060	0,009

Table 2 continued

No.	Numerical method	Numer of steps	Numer of calculations	δ_{i4} [%]	δ_{i5} [%]
7	AB III	296	296	0,035	0,008
8	RK IV	77	308	0,036	0,011
9	T	319	319	0,031	0,016
10	ABM III	171	342	0,036	0,009
11	NŚ I	344	344	0,031	0,012
12	G IV	231	462	0,042	0,009
13	BS	154	462	0,033	0,007
14	G III	268	536	0,033	0,009
15	RKF 23	157	628	0,033	0,007
16	AB II	715	715	0,035	0,014
17	ABM II	365	730	0,030	0,014
18	RK II	472	944	0,034	0,013
19	G II	693	1386	0,029	0,015

4. AN EXAMPLE OF THE APPLICATION OF THE DESCRIBED METHOD FOR THE ANALYSIS OF AC CIRCUIT

In this part of the paper, an algorithm is presented to solve AC circuits using the method of average voltage on the integration step length. This analysis method is basing on the electrical circuit shown in Fig. 7 which forms a part of the phase conductor for a three-phase 400 kV high-voltage network. In the analysis, the following data was adopted: the resistance and inductance of the R_S = 0.5Ω, L_S = 31.831 mH, the parameters of a long line of resistance unit R'_L = 0.0288 Ω/km, inductance L'_L = 1.0287 mH/km, capacity C'_{L1} = 5,616 nF/km C'_{L2} = 5.616 nF/km, length l = 108 km, resistance and inductance of the load R_0 = 4700 Ω, L_0 = 8.913 H, voltage $e(t)$ = 330000sin(2π·f·t) [11].
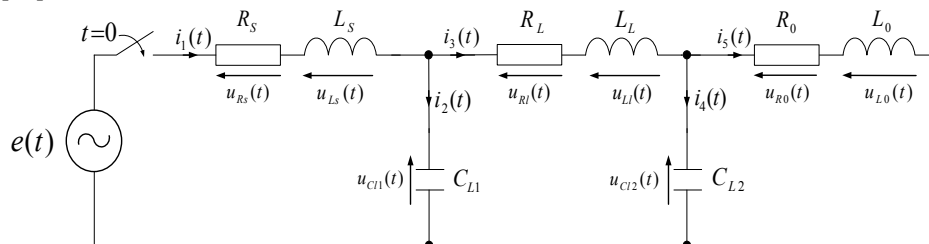

Fig. 7. The diagram of the analyzed AC circuit

The first step is to replace each branch with the serial connection of an equivalent E_S electromotive force and the equivalent R_S resistance.
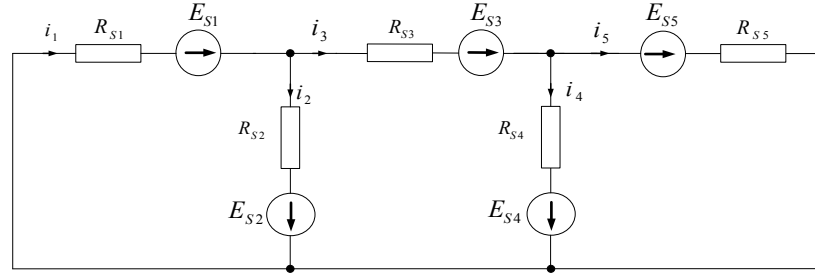
Fig. 8. The equivalent diagram of the analyzed AC circuit

The equivalent diagram of the analyzed circuit is shown in Fig. 8. Such electrical circuit can be described on the basis of 1st and 2nd Kirchhoff's Right with the following system of equations:

$$R_{S1}i_{11} + R_{S2}i_{21} = E_{S1} + E_{S2}$$

$$R_{S2}i_{21} - R_{S3}i_{31} - R_{S4}i_{41} = E_{S2} - E_{S3} - E_{S4}$$

$$R_{S4}i_{41} - R_{S5}i_{51} = E_{S4} - E_{S5}$$

$$i_{21} = i_{11} - i_{31} \qquad i_{41} = i_{31} - i_{51}$$

(8)

The above equations, after simplification, can be written as the following system of equations:

$$(R_{S1} + R_{S2}) \cdot i_{11} - R_{S2}i_{31} = E_{S1} + E_{S2}$$

$$R_{S2}i_{11} - (R_{S2} + R_{S3} + R_{S4}) \cdot i_{31} + R_{S4}i_{51} = E_{S2} - E_{S3} - E_{S4}$$

$$R_{S4}i_{31} - (R_{S4} + R_{S5}) \cdot i_{51} = E_{S4} - E_{S5}$$

$$i_{21} = i_{11} - i_{31} \qquad i_{41} = i_{31} - i_{51}$$

(9)

The algorithm for solving the electrical circuit shown in Fig. 8 has been presented for the method of average voltage on the integration step length of the 3rd order (coefficient m occurring in the general formulas (1), (2) and (4) assumes a value of 3).
1. Determination of the first derivatives at the beginning of the integration step. Derivatives should be recorded on the basis of an electrical circuit diagram shown in Fig. 7 as follows:

$$\frac{di_{10}}{dt} = \frac{330000 \cdot \sin(2\pi \cdot f \cdot t_0) - R_S i_{10} - R_2 i_{20} - u_{CL10}}{L_S}$$

$$\frac{di_{30}}{dt} = \frac{u_{CL10} - u_{CL20} + R_L i_{30}}{L_L} \qquad \frac{di_{50}}{dt} = \frac{u_{CL20} - R_0 i_{50}}{L_0}$$

$$\frac{di_{20}}{dt} = \frac{di_{10}}{dt} - \frac{di_{30}}{dt} \qquad \frac{di_{40}}{dt} = \frac{di_{30}}{dt} - \frac{di_{50}}{dt}$$

2. Determination of the second derivatives at the beginning of the integration step. Derivatives should be recorded on the basis of an electrical circuit diagram shown in Fig. 7 as follows:

$$\frac{d^2 i_{10}}{dt^2} = \frac{2\pi \cdot f \cdot 330000 \cdot \sin(2\pi \cdot f \cdot t_0)}{L_S} - \frac{R_S}{L_S}\frac{di_{10}}{dt} - \frac{1}{L_S \cdot C_{L1}} i_{20}$$

$$\frac{d^2 i_{30}}{dt^2} = \frac{1}{L_L \cdot C_{L1}} i_{20} - \frac{1}{L_L \cdot C_{L2}} i_{40} - \frac{R_L}{L_L}\frac{di_{30}}{dt}$$

$$\frac{d^2 i_{50}}{dt^2} = \frac{1}{L_0 \cdot C_{L2}} i_{40} - \frac{R_0}{L_0}\frac{di_{50}}{dt}$$

$$\frac{d^2 i_{20}}{dt^2} = \frac{d^2 i_{10}}{dt^2} - \frac{d^2 i_{30}}{dt^2} \qquad \frac{d^2 i_{40}}{dt^2} = \frac{d^2 i_{30}}{dt^2} - \frac{d^2 i_{50}}{dt^2}$$

3. Calculating the values of equivalent electromotive E_S forces:

$$E_{S1} = \int_{t_0}^{t_0+\Delta t} \left(330000\sin\left(2\pi \cdot f \cdot t\right)\right)dt - R_S i_{10} +$$

$$+\left(\frac{R_S}{4} + \frac{L_S}{\Delta t}\right) \cdot i_{10} - \frac{R_S \Delta t}{4}\frac{di_{10}}{dt} - \frac{R_S \Delta t^2}{24}\frac{d^2 i_{10}}{dt^2}$$

$$E_{S2} = -u_{C10} - \frac{9\Delta t}{20 C_{L1}} \cdot i_{20} - \frac{7\Delta t^2}{60 C_{L1}} \cdot \frac{di_{20}}{dt} - \frac{\Delta t^3}{60 C_{L1}} \cdot \frac{d^2 i_{20}}{dt^2}$$

$$E_{S3} = -R_L i_{30} + \left(\frac{R_L}{4} + \frac{L_L}{\Delta t}\right) \cdot i_{40} - \frac{R_L \Delta t}{4}\frac{di_{30}}{dt} - \frac{R_L \Delta t^2}{24}\frac{d^2 i_{30}}{dt^2}$$

$$E_{S4} = -u_{C20} - \frac{9\Delta t}{20 C_{L2}} \cdot i_{40} - \frac{7\Delta t^2}{60 C_{L2}} \cdot \frac{di_{40}}{dt} - \frac{\Delta t^3}{60 C_{L2}} \cdot \frac{d^2 i_{40}}{dt^2}$$

$$E_{S5} = -R_0 i_{50} + \left(\frac{R_0}{4} + \frac{L_0}{\Delta t}\right) \cdot i_{50} - \frac{R_0 \Delta t}{4}\frac{di_{50}}{dt} - \frac{R_0 \Delta t^2}{24}\frac{d^2 i_{50}}{dt^2}$$

4. Calculation of the equivalent R_S resistance, using the formula (2):

$$R_{S1} = \frac{R_S}{4} + \frac{L_S}{\Delta t} \; ; \; R_{S2} = \frac{\Delta t}{20 C_{L1}} \; ; \; R_{S3} = \frac{R_L}{4} + \frac{L_L}{\Delta t} \; ; \; R_{S4} = \frac{\Delta t}{20 C_{L2}} \; ; \; R_{S5} = \frac{R_0}{4} + \frac{L_0}{\Delta t}$$

5. The solution of equation (9). On this basis the current values at the end of the current integration step are obtained.

6. Determination of voltages on the capacitors at the end of the integration step using the formula (4):

$$u_{CL11} = u_{CL10} + \frac{\Delta t}{4C_{L1}} \cdot (3 \cdot i_{20} + i_{21}) + \frac{\Delta t^2}{4C_{L1}} \frac{di_{20}}{dt} + \frac{\Delta t^3}{24C_{L1}} \frac{d^2 i_{20}}{dt^2}$$

$$u_{CL21} = u_{CL20} + \frac{\Delta t}{4C_{L2}} \cdot (3 \cdot i_{40} + i_{41}) + \frac{\Delta t^2}{4C_2} \frac{di_{40}}{dt} + \frac{\Delta t^3}{24C_2} \frac{d^2 i_{40}}{dt^2}$$

The analysis of the given system in the time-domain consisted of determining the transient currents $i_1(t)$, $i_2(t)$, $i_3(t)$, $i_4(t)$, $i_5(t)$. Transient currents $i_1(t)$ and $i_2(t)$, are shown in Fig. 9. The transient currents were obtained by solving the system of equations analytically and numerically with a fixed time step. The following methods were used: [1, 2, 3, 4, 5, 6, 7, 10]:

- trapezoids (T),
- 4th order Runge-Kutta f (RKIV)
- Bogacki-Shampine (BS),
- 4th and 5th order Dormand-Prince (DP54),
- 2nd and 3rd order Runge-Kutta-Fehlberg (RKF23),
- 4th and 5th order Runge-Kutta-Fehlberga(RKF45),
- 3rd order Adams-Bashfortha (ABIII),
- 4th order Adams-Bashforth (ABIV),
- 3rd order Adams-Moulton-Bashfortha (ABMIII),
- 4th order Adams-Moulton-Bashforth (ABMIV),
- 3rd order Gear (GIII),
- 4th order Gear IV (GIV),
- 1st order method of average voltage on the integration step length (NSI)
- 2nd order method of average voltage on the integration step length (NŚII),
- 3rd order method of average voltage on the integration step length (NŚIII).

The error was determined from the equation (7). It was assumed that the maximum value may equal 0.500%.

Tables 3 and 4 present the results of the analyzed circuit simulation, which inform about how many steps, in the given method, you need to perform during the occurrence of the transient state in order to obtain a solution with a predetermined maximum error (parameter labeled "number of steps"), and how many calculations you need to perform during the occurrence of the transient state in order to obtain a solution with a predetermined maximum error. This indicates the time of designation, given that the number of calculations is the product of the number of steps in the method which must be performed by the number of coefficients calculated in the method, which are needed to determine the next value ("Calculation volume" parameter).

Table 3. Simulation results for the given AC circuit

No.	Numerical method	Number of steps	Number of calculatios	δ_{i1} [%]	δ_{i2} [%]	δ_{i3} [%]
1	NŚ III	5651	16953	0,186	0,500	0,112
2	AB IV	23500	23500	0,191	0,500	0,119
3	ABM IV	13381	26762	0,186	0,500	0,112
4	NŚ II	13710	27420	0,191	0,500	0,119
5	RKF 45	4613	27678	0,188	0,500	0,115
6	DP 54	5349	32094	0,186	0,500	0,112
7	RK IV	9243	36972	0,190	0,500	0,119
8	G IV	20220	40440	0,185	0,500	0,111
9	ABM III	25080	50160	0,191	0,500	0,119
10	AB III	51699	51699	0,192	0,500	0,120
11	BS	24875	74625	0,192	0,500	0,120
12	NŚ I	76300	76300	0,204	0,500	0,138
13	G III	44750	89500	0,191	0,500	0,119
14	RKF 23	25291	101164	0,192	0,500	0,120
15	T	107900	107900	0,204	0,500	0,138

Table 4. Simulation results for the given AC circuit

| No.	Numerical method	Number of steps	Number of calculatios	δ_{i4} [%]	δ_{i5} [%]
1	NŚ III	5651	16953	0,117	0,005
2	AB IV	23500	23500	0,124	0,005
3	ABM IV	13381	26762	0,117	0,005
4	NŚ II	13710	27420	0,124	0,005
5	RKF 45	4613	27678	0,120	0,005
6	DP 54	5349	32094	0,117	0,005
7	RK IV	9243	36972	0,124	0,005
8	G IV	20220	40440	0,116	0,005
9	ABM III	25080	50160	0,125	0,005
10	AB III	51699	51699	0,127	0,005
11	BS	24875	74625	0,126	0,005
12	NŚ I	76300	76300	0,145	0,006
13	G III	44750	89500	0,125	0,005
14	RKF 23	25291	101164	0,126	0,005
15	T	107900	107900	0,145	0,006
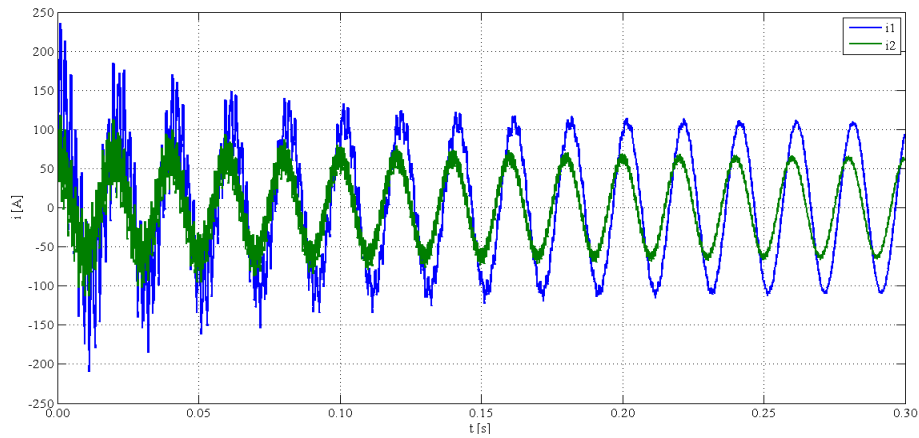
Fig. 9. The analytically designated transient currents i_1 and i_2 flowing in the analyzed AC circuit
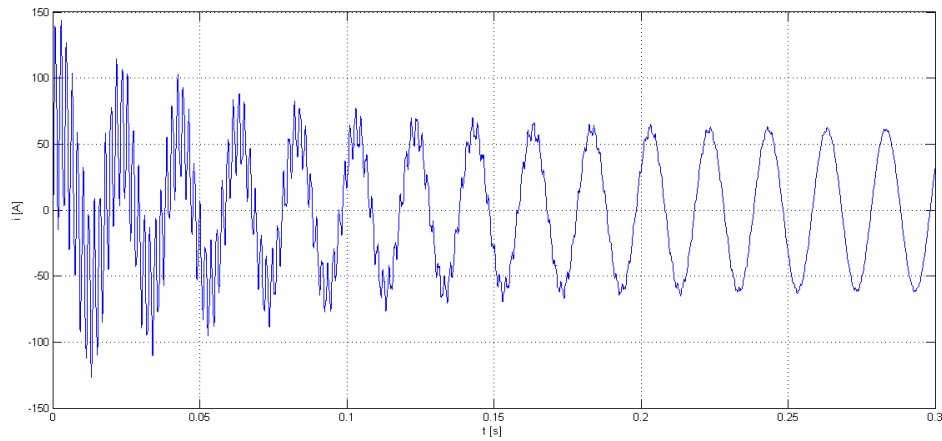

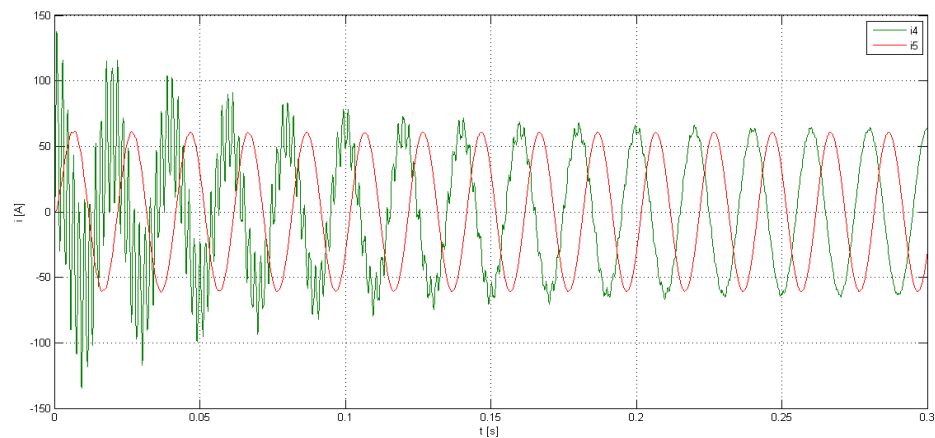Fig. 10. The analytically designated transient current i_3 flowing in the analyzed AC circuit

Fig. 11. The analytically designated transient currents i_4 and i_5 flowing in the analyzed AC circuit

5. GENERAL GUIDELINES FOR THE USAGE OF THE GIVEN METHOD FOR THE ANALYSIS OF COMPLEX ELECTRICAL CIRCUITS

Method of average voltage on the integration step length provides the algebraization of equations, so that the electrical circuit refers on the integration step to the diagram used in the DC circuit analysis.

Electrical circuit analysis procedure is as follows:

1. The selection of methods of appropriate order (the authors suggest the method of the second order, $m = 2$)
2. The creation of an equivalent diagram on the basis of the analyzed system;
3. The formulation of equations based on Kirchhoff's laws or method of loop currents and nodal potentials for the equivalent diagram;
4. The formulation of equations to determine the parameters of the branch circuit replacement E_S and R_S or J_S and G_S (these parameters are calculated based on the initial conditions at the beginning of the integration step for the analyzed scheme);
5. The calculation of the currents at the end of the integration step (solving the system of equations formulated in Section 3 with Item 4);
6. The calculation of the voltage on the capacitors at the end of the integration step;
7. The adoption of calculations of points 5 and 6 as the initial conditions for the next step.

It is worth stressing that, in the nodes of the equivalent electrical circuit, currents add up at the end of the integration step, and average voltages appear between the nodes on the integration step length.

6. CONCLUSIONS

After analyzing the results shown in tables 1 and 2, it can be concluded that for the electrical current circuit (Fig. 4) and alternating current (Fig. 7) the transient currents with predetermined errors were imitated in all numerical methods used in this paper.

Analyzing the results presented in tables 1 and 2 for the analyzed circuit, including the number of steps performed during the occurrence of the transient in the analyzed circuits and the number of coefficients calculated by defining the next approximations, it can be concluded that methods such as:

- The 3rd order method of average voltage on the integration step length
- The 4th order Adams – Bashforth method,
- The 4th order Adams – Bashfothra – Moulton method
- The 2nd order method of average voltage on the integration step length

allow to obtain the solution faster, in comparison to the other methods.

The presented results included in Table 1 and 2 show that the multistep methods (the 4th order Adams – Bashforth method and the 4th order Adams – Bashfothra – Moulton method) obtain, in a relatively quick way, a solution with a predetermined accuracy. The disadvantage of multistep methods is that they are not self-steering i.e. they cannot be used at the beginning of the calculation. In order to reach a solution with these methods, the calculations need to be started with the use of one-step methods, which affect the number of calculations in the entire simulation period. The method presented in this paper does not have this disadvantage.

To summarize, it can be stated that while considering complex circuits, the fastest method of obtaining the solution with predetermined error is the method of average voltage on the integration step length, in comparison with conventional numerical methods.

BIBLIOGRAPHY

[1] Arieh Iserles, 2008. A First Course in the Numerical Analysis of Differential Equations. Cambridge Texts in Applied Mathematics.
[2] Cleve B. Moler, 2004. Numerical Computing with MATLAB. The MathWorks, Inc., Natick, Massachusets.
[3] David F. Griffiths, Desmond J. Higham, 2010. Numerical Methods for Ordinary Differential Equations: Initial Value Problems. Springer.
[4] Dommel H.W., 1969. Digital computer solution of elektromagnetic trasients in single- and multiphase networks.
[5] Dormand J.R., Prince P.J., 1980. Family of embedded Runge – Kutta formulae. Journal of Computational and Applied Mathematics 6(1A).
[6] Kincaid D., Chney W., 2006. Analiza numeryczna. WNT Warszawa.
[7] Mathews J.H., Fink K.D., 1999. Numerical Methods using Matlab, Prentice Hall, Upper Saddle River New Jersey.
[8] Płachtyna O., Kłosowski Z., Żarnowski R., 2011. Ocena skuteczności metody napięć średniokrokowych w porównaniu z klasycznymi metodami całkowania numerycznego w modelach matematycznych obwodów elektrycznych, Kwartalnik Elektryka 1, Gliwice.
[9] Płachtyna O., Kłosowski Z., Żarnowski R., 2011. Model matematyczny napędu prądu stałego w oparciu o metodę średnich napięć na długości kroku całkowania, Przegląd Elektrotechniczny 12a.
[10] Rosłoniec S., 2008. Wybrane metody numeryczne z przykładami zastosowań w zadaniach inżynierskich, Wyd. Politechniki Warszawskiej Warszawa.
[11] Rosłowski E., 2009. Komputerowe metody analizy elektromagnetycznych stanów przejściowych, Wyd. Politechniki Wrocławskiej Wrocław.

ZASTOSOWANIE METODY ŚREDNICH NAPIĘĆ NA DŁUGOŚCI KROKU CAŁKOWANIA DO ANALIZY OBWODÓW ELEKTRYCZNYCH

Streszczenie

W artykule przedstawiono analizę złożonych obwodów elektrycznych z wykorzystaniem metody średnich napięć na długości kroku całkowania. Zaprezentowano algorytm rozwiązywania prezentowaną metodą złożonych obwodów elektrycznych. W pracy dokonano również porównania czasów wyznaczania rozwiązania numerycznego różnymi metodami przy założonym błędzie między tym rozwiązaniem, a rozwiązaniem dokładnym. Porównanie to służy określeniu przydatności (skuteczności) danej metody do analizowania złożonych obwodów elektrycznych.

Słowa kluczowe: analiza obwodów elektrycznych, metoda średnich napięć na długości kroku całkowania, porównanie złożoności metod całkowania numerycznego

INFLUENCE OF TITANIUM LAYER ON COUNTER ELECTRODE ON ELECTRICAL PARAMETERS OF DSSC

Wojciech Wachowiak[1], Maciej Klein[3,4], Łukasz Skowroński[2]

[1]Institute of Electrical Engineering
[2]Institute of Mathematics and Physics
University of Technology and Life Sciences
al. prof. S. Kaliskiego 7, 85-796 Bydgoszcz, Poland
wojciech.wachowiak@utp.edu.pl

[3]Department of Physics of Electronic Phenomena, Gdansk University of Technology,
Narutowicza 11/12, 80-233 Gdansk, Poland

[4]Centre for Plasma and Laser Engineering,
Institute of Fluid-Flow Machinery, Polish Academy of Science,
Fiszera 14, 80-231 Gdansk, Poland

Summary: In this paper the influence of the Ti layer thickness at counter-electrode on electrical parameters of DSSCs was examined. The transparent conductive oxide – less (TCO-less) counter electrodes (CE) with titanium layers and platinum as catalyst on Bk7 glass were prepared. Thin metallic films were deposited by means of magnetron sputtering (titanium) and Pulsed Laser Deposition (platinum). The counter electrode with Pt layer on Fluorine doped Tin Oxide (FTO) were used as reference PV cells. The obtained results indicated that the Ti coated cathodes may be used in transparent conductive oxide – less (TCO-less) dye sensitized solar cells as an alternative for Pt/FTO system.

Keywords: DSSC, counter-electrode, TCO-less, titanium layers

1. INTRODUCTION

Dye Sensitized Solar Cells (DSSC) belongs to III generation of photovoltaic cells. They emerge as one of the cheapest solution in terms of acquiring electrical energy from photovoltaic conversion.

In their basic configuration the DSSC consist of glass transparent and conductive electrode, the TiO_2 layer with adsorbed dye on its surface, electrolyte and counter electrode covered with catalytic layer [1]. Presently, many studies on using different materials as a CE are conducted. Because of their low price, high conductivity, scalability and corrosion resistance the titanium, titanium nitride or steel is used as a conductive material in CE. These materials are used in various forms such as thin films [2,7,9], foils [3,5,9,15], grids [11,14] or plates [4,7,8].

Basically, the sunlight to electric energy conversion in the DSSC occurs when an incident radiation (photons) are absorbed by the photosensitive dye adsorbed on semiconductor surface. As a result, dye molecules passing from the ground state S^o to excited state S^* [6]:

$$S^o + hv \rightarrow S^*. \tag{1}$$

The excited electron is injected into the conduction band of titanium dioxide, leaving the dye molecule in the oxidized state S^+:

$$S^* \rightarrow S^+ + e^- (TiO_2). \tag{2}$$

The injected electron diffuses through the semiconductor layer to the conductive film deposited on a glass substrate and from there trough the external load to the counter electrode Eq.(3). The oxidized dye molecule S^+ accepts the electron from redox ion I^- and returns to the basic state S^o whereas I^- is oxidized to I^-_3:

$$2S^+ + 3 I^- \rightarrow 2S^o + I^-_3. \tag{3}$$

The cycle is ended by I^-_3 ion, which diffuses to counter electrode and is reduced to the I^- ion:

$$I^-_3 + 2e^-(Pt) \rightarrow 3 I^-. \tag{4}$$

Described mechanism of the electric charge carriers transfer in DSSCs is schematically presented in Fig. 1.
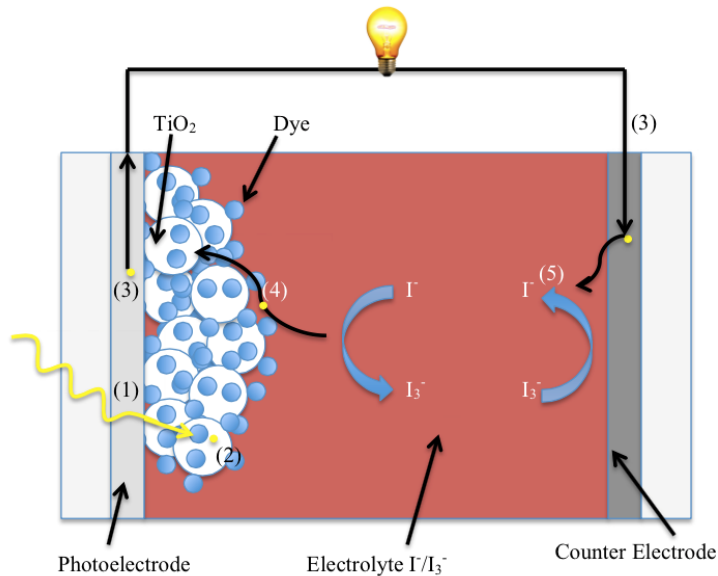

Fig 1. The Dye Sensitized Solar Cell construction and principle of operation

The DSSC can be presented in the form of a simplified electric circuit, which consists a current source and two resistances: a sheet resistance (R_s) and a shunt resistance (R_p) – Fig. 2.
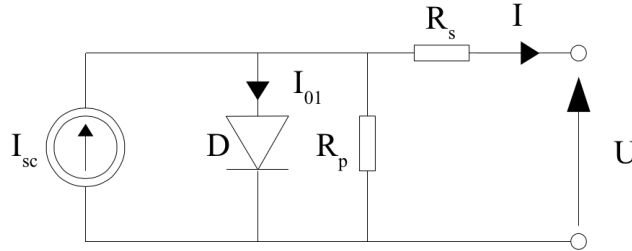
Fig. 2. An electrical circuit of the photovoltaic cell

Electrical parameters characterizing the solar cell are described below:

- η – the photoconversion efficiency; determines maximum ratio of the power developed on cell's electrodes to power of incident sunlight;
- I_{SC} – the short circuit current; the maximum current generated by photovoltaic cell in the short circuit condition ($U = 0$);
- U_{OC} – the open circuit voltage; occurring when there is no current flow ($I = 0$);
- P_{max} – the maximum power generated on photovoltaic cells electrodes when the load resistance is equal to internal resistance of the cell.
- FF – the fill factor; describes I-V characteristic shape;
- R_s and R_p – sheet and shunt resistance.

The fill factor (FF) is described by the following equation:

$$FF = \frac{P_{max}}{U_{oc}I_{sc}} = \frac{U_{max}I_{max}}{U_{oc}I_{sc}} \cdot 100\% \, . \tag{5}$$

U_{max}, I_{max}, I_{SC} and U_{OC} quantities are schematically shown in Fig. 3.
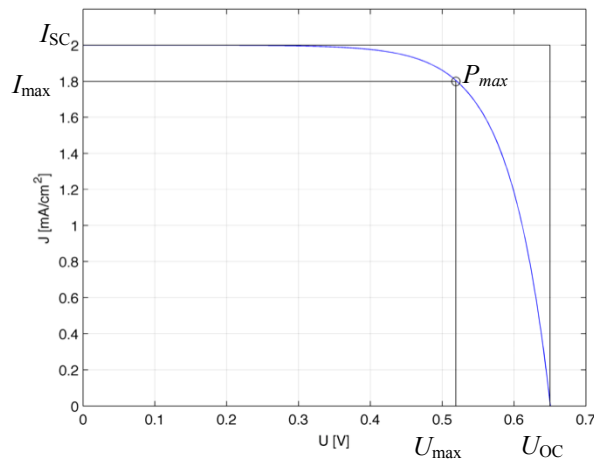

Fig. 3. Graphical representation of fill factor coefficient

The aim of this paper was to investigate the influence of counter electrode type on I-V characteristics of Dye Sensitized Solar Cells and their electrical parameters. Counter electrodes where prepared on the Bk7 glass substrate with variable thickness of the Ti layer, deposited by means of the magnetron sputtering. Titanium layers were coated with thin platinum layer (as a catalyst) deposited using the pulse laser deposition (PLD) method. The reference counter electrode was prepared by deposition Pt thin film on the FTO glass substrate.

2. EXPERIMENTAL DETAILS

Measurements of I-V characteristics were recorded under standard test conditions, i.e. the cell temperature $25^{\circ}C$, AM 1.5 solar spectrum and irradiance 1000 W/m^2. As the light source the XBO 150 W (Optel) xenon lamp, equipped with optical IR and AM 1.5 filters, were used. Radiation intensity was calibrated using a light meter (Ophir).

Current-voltage characteristics of the solar cells were recorded using the current-voltage source Keithley 2400, connected to the PC via the serial interface RS-232C and RS-232C/USB adapter (Fig. 4).
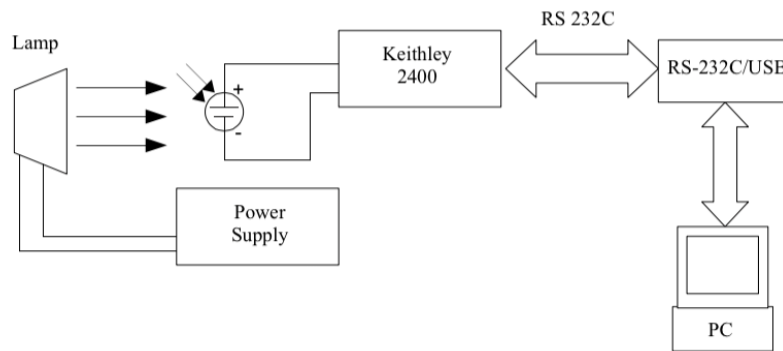

Fig. 4. Schematic diagram of the I-V characteristics measurement system

The program used to record the current-voltage characteristics of photovoltaic cells was implemented in LabView. It uses a serial interface to communicate with the Keithley 2400 device (VISA standard, SCPI command language). For the I-V characteristics registration, the linear voltage sweep method was used. The current measurement was performed for specific voltage steps. The main parameters for this method are: initial and final values, number of steps and time delay (a time between voltage setting and measurement). For a constant step length increase of the applied voltage is linear. The measurement system scheme is shown in Fig. 5.
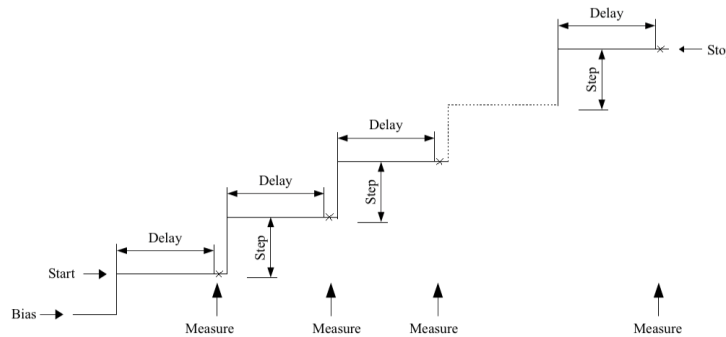
Fig. 5. The linear voltage sweep method of recording the I-V characteristics

Analysis of recorded current-voltage characteristics (determination of the I_{sc}, U_{oc}, P_{max}, I_{max}, U_{max}, FF and η parameters) was performed using the program implemented in Matlab.

3. SAMPLE PREPARATION

3.1. SUBSTRATE

As the substrate for counter electrodes, the Bk7 glass (Menzel-Glasser) and glass coated with FTO (Aldrich) were used. The substrates were cleaned by successively placing them in an ultrasonic bath (15 minutes each bath) with the following solutions: a distilled water, acetone, ethanol and isopropanol and drying in a stream of compressed pure air.

3.2. COUNTER ELECTRODE

The following counter electrodes were prepared:
- the Ti conductive layer deposited on Bk7 and FTO substrates; the platinum film was used as a catalyst (two thicknesses of Pt).
- the Ti layer with a variable thickness deposited on the Bk7 substrate and platinum film as a catalyst..

The titanium layers were deposited using the gas injection magnetron sputtering method (GIMS) [16]. The thickness of titanium layer was adjusted by varying the speed of substrate passing under targets (v), number of cycles (k) and the number of used targets (t). The deposition process was carried out under a pressure of 10^{-2} Pa (an initial pressure). The Ar gas was used as a sputter gas and was injected by the flow of 450 sccm.

Platinum layers were deposited by means of PLD at the Institute of Fluid-Flow Machinery of Polish Academy of Sciences in Gdansk [1]. As the radiation source, the nanosecond pulse Nd:YAG laser (Quantel) was used. The energy of a single pulse was 32 mJ with a repetition rate 10 Hz. The distance between the substrate and the target was 4.5 cm. Deposition of the Pt layers was carried out under a pressure of 5.4 10^{-3} Pa.

The deposition time was 1.5 minutes or 2 minutes. Table 1 shows used substrates, technological parameters of the magnetron sputtering process used to deposit Ti layers and the thickness of metallic film (d) [10]. Table 1 contains 4 samples for which results were presented and discussed earlier in a separate monograph [12] and are added to complete the analysis.

Table 1. Technological parameters used to deposit titanium layers

Sample	Substrate	v (cm/s)	k	t	d (nm)
Pt/Ti(315)/Bk7[1]	Bk7	0,68	2	3	315
Pt/Ti(41)/Bk7_1[1]	Bk7	1,36	1	1	41
Pt/Ti(315)/FTO[1]	FTO	0,68	2	3	315
Pt/Ti(41)/FTO[1]	FTO	1,36	1	1	41
Pt/Ti(41)/Bk7_2	Bk7	1,36	1	1	41
Pt2/Ti(41)/Bk7	Bk7	1,36	1	1	41
Pt/FTO	FTO	-	-	-	-
Pt2/FTO	FTO	-	-	-	-
Pt/Ti(41)/Bk7_3	Bk7	1,36	1	1	41
Pt/Ti(82)/Bk7	Bk7	1,26	1	2	82
Pt/Ti(183)/Bk7	Bk7	0,34	1	2	183
Pt/Ti(577)/Bk7	Bk7	0,136	1	2	577

[1] Results were presented earlier in a monograph [12]
Pt and Pt2 means thinner (a deposition time was 1.5 min) and thicker (a deposition time was 2 min) platinum layer, respectively

3.3. PHOTOELECTRODE

The photoanode was prepared by the deposition of mesoporous TiO_2 layer applying *doctor blade* method [1]. The surface was reduced using Scotch tape (3M). Prepared films were subjected to calcination in the furnace chamber (Midisun, Neoterm) at 450 °C for 30 min. in air atmosphere (a heating rate 10 °C/min.). During cooling, when the temperature reaches approx. 80 °C, the electrode was immersed in a 0.5 mM solution of the N3 dye (Solaronix) dispersed in a dry ethanol and was stored for 24 h in a protected from light place at a room temperature. After removing from the solution the electrode was washed in a dry ethanol and dried in a stream of a hot air to remove excess of a dye.

3.4. ELECTROLYTE

The electrolyte was a 0.5 M solution of 4-tert-butylpiridine (Aldrich), 0.1 M guanidine thiocyanate (Aldrich), 0.6 M 1-propyl-3-methyl-imidazolium iodide (Aldrich) and 0.03 M iodine (POCH) in acetonitrile [13]. Both electrodes were connected by a sealing foil with a thickness of 60 microns (Meltonix, Solaronix). The complete cells are shown in Fig. 6.
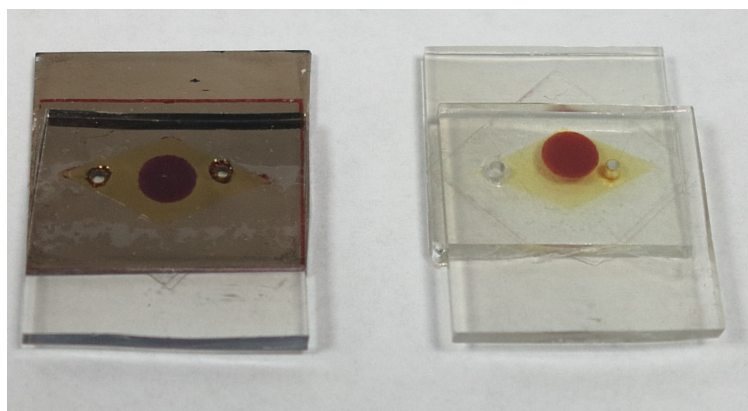
Fig. 6. The TCO-less Dye Sensitized Solar Cell (left) and reference DSSC (right)

4. RESULTS AND DISCUSSION

Fig. 7 presents series of I-V characteristics for DSSCs with Pt/Ti system as a counter electrode with two different thickness of the titanium film deposited on both the Bk7 glass and FTO coated glass substrates. Table 2 contains determined electrical parameters (I_{sc}, U_{oc}, P_{max}, I_{max}, U_{max}, FF and η) of all examined DSSCs. It can be concluded that electrical characteristics of cells depend on the thickness of titanium layer and substrate (Bk7, FTO). Generally, the higher fill factor (FF) and efficiency (η) were obtained for systems with a thick layer of Ti deposited directly onto a Bk7 glass. For the sample Pt/Ti(315)/Bk7 the fill factor (FF) and efficiency (η) are 0.52 and 4.0%, respectively. For the same system but with a thin titanium layer the values of FF and η parameters are about one-fourth lower ($FF = 0.37$, $\eta = 2.9\%$).

For the cells with Pt/Ti system deposited on FTO the behavior of electrical parameters was reversed. Higher values of fill factor (FF) and efficiency (η) were obtained for system with thinner Ti layer: 0.41 and 3.5 respectively, and lower for the thick layer ($FF = 0.38$, $\eta = 2.4\%$).

Fig. 8 presents characteristics of cells prepared for testing the effect of different platinum amount on the counter electrode on electric parameters of DSSCs. The results were compared with the results for cells without a titanium layer - a standard Pt/FTO counter electrode was used in a reference DSSC. These characteristics indicate that there are no large differences between the properties of individual cells. Increasing deposition time of catalyst (Pt) by 30% did not result in a significant improvement of the electrical parameters of DSSCs.

Fig. 9 shows the current-voltage characteristics of DSSCs with different thicknesses of titanium on the counter electrode. The analysis of the above results leads to a conclusion that there is an optimum thickness of the Ti layer for which maximum efficiency of the cell can be achieved. An increase of the maximum power (P_{max}), fill factor (FF) and efficiency (η) can be seen with increasing thickness of the Ti for the first three samples. For DSSC with the thicker Ti layer a decrease of the maximum power from 3.2 mW (Pt/Ti(183)/Bk7) to 2.9 mW (Pt/Ti(577)/Bk7) was observed. The highest photoelectric conversion efficiency (2.6%) in this group of cells was obtained

for Pt/Ti(183)/Bk7 sample. Moreover, this sample is characterized by the highest fill factor (*FF*), with value is 0.64. It should be noted that this is the highest value of *FF* for all of the produced DSSCs in this study.
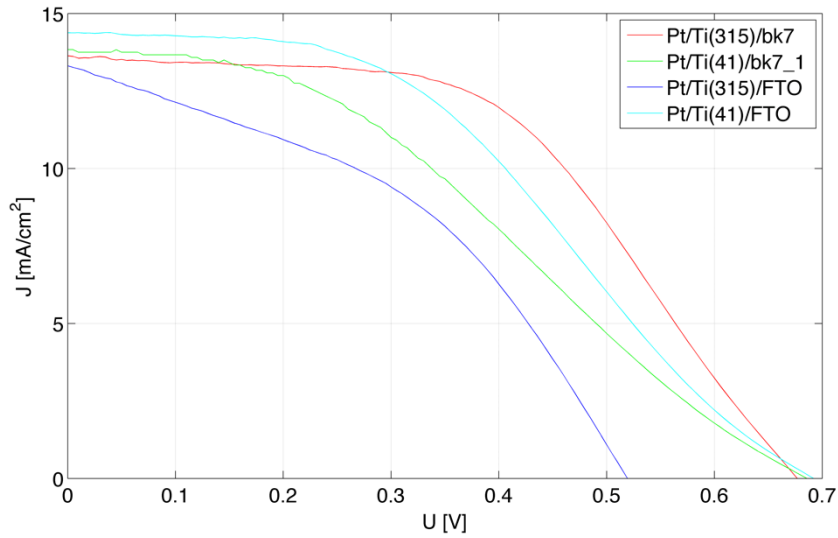

Fig. 7. I-V characteristics of DSSC with a different substrate

Table 2. Electrical parameters of examined DSSC

| Sample	J_{sc} (mA/cm^2)	U_{oc} (V)	P_{max} (mW)	J_{max} (mA/cm^2)	U_{max} (V)	*FF*	η (%)
Pt/Ti(315)/Bk7[1]	13,85	0,67	4,807	11,45	0,42	0,51	4,0
Pt/Ti(41)/Bk7_1[1]	13,99	0,68	3,488	10,26	0,34	0,37	2,9
Pt/Ti(315)/FTO[1]	14,48	0,52	2,869	8,69	0,33	0,38	2,4
Pt/Ti(41)/FTO[1]	14,65	0,69	4,176	11,29	0,37	0,41	3,5
Pt/Ti(41)/Bk7	13,08	0,68	3,406	9,73	0,35	0,38	2,7
Pt2/Ti(41)/Bk7[2]	13,60	0,69	3,525	10,22	0,35	0,37	2,8
Pt/FTO	14,24	0,65	3,478	10,38	0,34	0,37	2,8
Pt2/FTO[2]	14,07	0,65	3,575	10,83	0,33	0,39	2,9
Pt/Ti(41)/Bk7	8,88	0,62	2,636	6,94	0,38	0,48	2,1
Pt/Ti(82)/Bk7	7,63	0,63	2,810	6,69	0,42	0,58	2,3
Pt/Ti(183)/Bk7	8,23	0,62	3,224	7,16	0,45	0,64	2,6
Pt/Ti(577)/Bk7	7,71	0,62	2,867	6,37	0,45	0,60	2,3
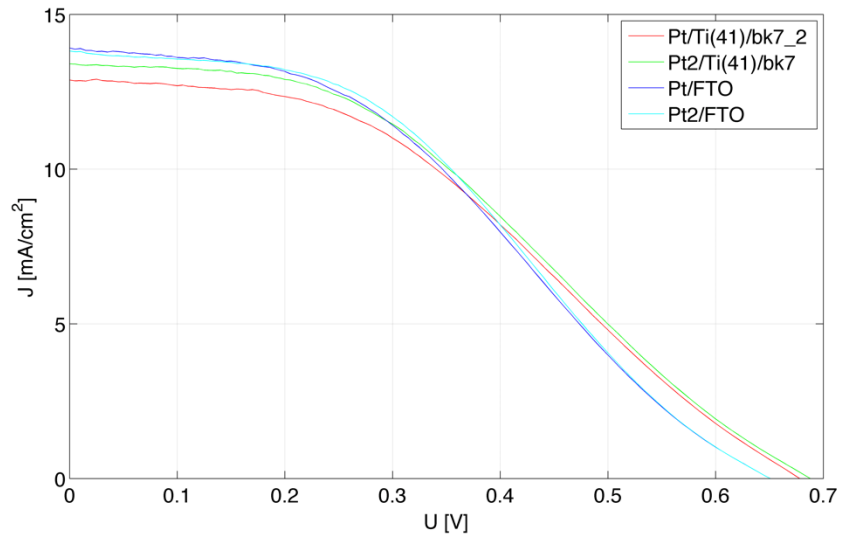
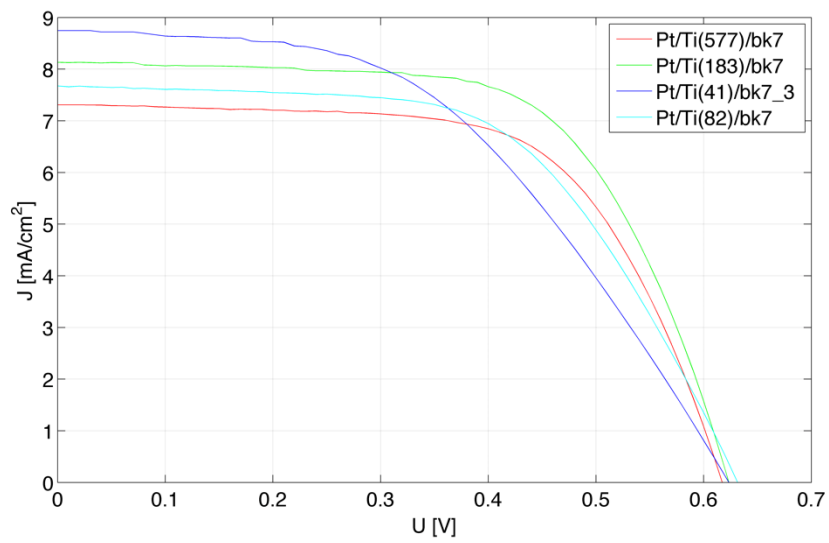Fig. 8. I-V characteristics of DSSC with different the Pt layer thickness

Fig. 9. I-V characteristics of DSSC with a different titanium layer thickness

5. CONCLUSION

The subject of this study was the influence of variable Ti and Pt layers thickness on the counter electrode and type of the substrate on electrical parameters of the TCO-less DSSCs. The best result was obtained for cell composed of the titanium layer (315 nm) deposited directly on the glass with the platinum film as a catalyst. The results indicate that the photocathode with the Ti layer may be used in dye sensitized solar cells containing only one transparent conductive electrode i.e. TCO-less Pt/Ti/Bk7 counter electrodes can replace standard Pt/FTO cathodes in DSSCs.

BIBLIOGRAPHY

[1] Górski M., Siudak K., Sibiński M., 2013. Elektrody z węgla szklistego oraz z platyny otrzymane metodą PLD dla barwnikowych ogniw fotowoltaicznych. Elektronika 5, 12-15.
[2] Hea J., Duffy N.W., Pringlea J.M., Chenga Y.-B., 2013. Conducting polymer and titanium carbide-based nanocom-posites as efficient counter electrodes for dye--sensitized solar cells, Electochimica Acta 105, 275-281.
[3] Kanga M.G., Parka N.-G., Ryua K.S., Changa S.H., Kimb K.-J., 2006. A 4.2% efficient flexible dye-sensitized TiO2 solar cells using stainless steel substrate. Solar Energy Materials and Solar Cells 90, 574-581.
[4] Kumara G.R.A., Kawasaki S., Jayaweera P.V.V., Premalal E.V.A., Kaneko S., 2012. Large area dye-sensitized solar cells with titanium based counter electrode. Thin Solid Films 520, 4119-4121.
[5] Lina L.-Y., Leea C.-P., Vittala R., Ho K.-C., 2010. Selective conditions for the fabrication of a flexible dye-sensitized solar cell with Ti/TiO2 photoanode. Journal of Power Sources 195, 4344-4349.
[6] Luque A., Hegedus S., 2003. Handbook of Photovoltaic Science and Engineering. Wiley, Chichester.
[7] Menga L., Wuc M., Wangd Y., Guod W., Mae C., Mad T., Silva R., 2013. Effect of the compact ti layer on the efficiency of dye-sensitized solar cells assembled using stainless steel sheets. Applied Surface Science 275, 222-226.
[8] Onoda K., Ngamsinlapasathian S., Fujieda T., Yoshikawa S., The superiority of Ti plate as the substrate S. of dye-sensitized solar cells, Solar Energy Materials and Solar Cells, 91 (2007) 1176-1181.
[9] Ouyangand F.-Y., Tai W.-L., 2013. Enhanced corrosion resistance of tin-coated stainless steels for the application in flexible dye-sensitized solar cells. Applied Surface Science 276, 563-570.
[10] Stachowicz A.A., Wachowiak W., Skowroński Ł., 2014. Właściwości optyczne warstw tytanowych do zastosowania w barwnikowych ogniwach fotowoltaicznych. CAX'2014: Computer Aided Science and Engineering III, 37-46.
[11] Vijayakumar V., Pasquier A.D., Birnie III D.P., 2011. Electrical and optical studies of flexible stainless steel mesh electrodes for dye sensitized solar cells. Solar Energy Materials and Solar Cells 95, 2120-2125.

[12] Wachowiak W., Klein M. Stachowicz A., Skowroński Ł., 2014. Wpływ rodzaju przeciwelektrody na parametry elektryczne ogniw fotowoltaicznych. CAX'2014: Computer Aided Science and Engineering III, 47-56.

[13] Zalas M., Klein M., 2012. The Influence of Titania Electrode Modification with Lanthanide Ions Containing Thin Layer on the Performance of Dye-Sensitized Solar Cells, International Journal of Photoenergy, 1-8.

[14] Xiao Y., Wu J., Yue G., Lin J., Huang M., Fan L., Lan Z., 2011. Fabrication of high performance Pt/Ti counter electrodes on ti mesh for flexible large-area dye-sensitized solar cells, Electochimica Acta 58, 621-627.

[15] Yue G., Tan F., Li F., Chen C., Zhang W., Wu J., Li Q., 2014. Enhanced performance of flexible dye-sensitized solar cell based on nickel sulfide/polyaniline/ titanium counter electrode, Electochimica Acta 149, 117-125.

[16] Zdunek K., Nowakowska-Langier K., Dora J., Chodun R., 2013. Gas injection as a tool for plasma process control during coating deposition, Surface & Coatings Technology 228, 367-373.

WPŁYW WARSTWY TYTANU NA PRZECIWELEKTRODZIE NA PARAMETRY ELEKTRYCZNE DSSC

Streszczenie

W przedstawionej pracy zbadano wpływ grubości warstwy Ti na przeciwelektrodzie na parametry elektryczne DSSC. Przygotowano nieprzezroczyste przeciwelektrody typu Transparent Conductive Oxide – less z warstwami tytanu na szkle Bk7 oraz FTO i platyny jako katalizatora. Cienkie filmy zostały osadzane na przeciwelektrodach z zastosowaniem rozpylania magnetronowego (Ti) oraz metodą osadzania za pomocą impulsów lasera (ang. Pulsed Laser Deposition, PLD) (Pt). Ogniwa z przeciwelektrodą z warstwą Pt naniesioną bezpośrednio na FTO zostały wykorzystane jako układy referencyjne. Uzyskane wyniki wskazują, że przeciwelektrody z warstwą Ti mogą być stosowane w barwnikowych ogniwach fotowoltaicznych typu TCO-less jako alternatywa dla standardowego systemu Pt/FTO.

Słowa kluczowe: barwnikowe ogniwa fotowoltaiczne, DSSC, przeciwelektroda TCO-less, warstwy tytanu

Lista recenzentów prac opublikowanych w 2014 roku
Reviewers list publication published in 2014

Wojciech Jarzyna (Politechnika Lubelska)
Grażyna Jastrzębska (Politechnika Poznańska)
Mieczysław Ronkowski (Politechnika Gdańska)
Dariusz Świsulski (Politechnika Gdańska)
Grzegorz Wiczyński (Politechnika Poznańska)
Maciej Włodarczyk (Politechnika Świętokrzyska)